Facilitating Flip-Flop: How Small-Molecule Structure Influences Interactions with Living Bacterial Membranes

Marea J. Blake, Hannah B. Castillo, Anna E. Curtis, and Tessa R. Calhoun*

Department of Chemistry, University of Tennessee, Knoxville

E-mail: trcalhoun@utk.edu

Abstract

The first barrier a small molecule must overcome before trespassing into a living cell is the lipid bilayer surrounding the intracellular content. It is imperative, therefore, to understand how the structure of a small molecule influences its fate in this region. Through the use of second harmonic generation (SHG), we show how the differing degrees of ionic headgroups, conjugated system, and branched hydrocarbon tail disparities of a series of four styryl dye molecules influence the propensity to 'flip-flop' or to be further organized in the outer leaflet by the membrane. We show here that initial adsorption experiments match previous studies on model systems, however, more complex dynamics are observed over time. Aside from probe molecule structure, these dynamics also vary between cell species and can deviate from trends reported based on model membranes. Specifically, we show here that the membrane composition is revealed to be an important factor to consider for headgroup-mediated dynamics. Overall, the findings presented here on how structural variability of small molecules impacts their initial adsorption and eventual destinations within membranes in the context of living cells could have practical applications in antibiotic and drug adjuvant design.

Significance

Remediation of bacterial infections is a global predicament that is challenged by the prevalence of antibiotic resistant species and the limited progress in novel drug design and discovery. It is well known that the success of antibiotics relies on an initial interaction with the plasma membrane of the target bacteria regardless of the drug's mode of action. However, few robust empirical methods currently exist for tracking and quantifying the progression of the individual steps of permeation in living bacterial membranes. These steps are, broadly, 1) initial adsorption, 2) flipping of the molecule into the inner bilayer leaflet and 3) subsequent desorption tactics. Each event leading to plasma membrane penetration is imperative to isolate in order to understand their individual contribution to the overall infiltration process. More specifically, how the structure of the exogenous small molecules, and the membrane composition they are exposed to, impact these processes is a necessary direction to explore as slight modifications of chemical structure can pose differences in membrane interactions and further pharmacokinetic properties. To address this, the interface specificity of second harmonic generation, a nonlinear optical technique, is employed to reveal how structural variances among small molecules influence their affinity to and dynamics within living bacterial lipid bilayers.

Introduction

One of the most important natural interfaces is the cellular plasma membrane. This boundary between the cytoplasm and extracellular space is responsible for maintaining structural integrity, protecting the cell from environmental stressors, and mediating small molecule transport and signaling.[1,2] This latter role is especially important for efforts to combat antibiotic resistance as penetration into the cell has limited rational drug design.[3] The typical biological membrane is often portrayed as a heterogeneous, multidimensional unit composed primarily of a phospholipid bilayer - equipped with a hydrophobic core and hydrophilic ex-

terior - with proteins and cytoskeletal components interspersed throughout. Moreover, lipid membrane architecture is one of the characteristics that defines a living system. For instance, the presence of membrane-bound organelles differentiates a eukaryotic cell from a bacterium, and having a single or double membrane present discerns between Gram-positive and Gram-negative bacteria classifications. Although cell types can be generally classified by their membrane design, the membranes between individual species, and even among strains of the same species, differ drastically in composition and organization. For instance, although *Staphylococcus aureus* and *Bacillus subtilis* are both Gram-positive bacteria, their carotenoid content and phospholipid headgroup/tail compositions vary drastically, imposing significant differences in membrane organization.[1,4–6] This compositional difference between bacterial species can consequently result in contrasting interactions with small molecules, including antibiotics.[7–9]

Further, the lipid bilayer is an ever-changing landscape in which the components can alter their arrangement and composition in response to environmental cues such as changes in pH, temperature, and the presence of ions, fatty acids, and small molecules in the cells' surroundings.[1,10–12] In some cases, this characteristic imparts drug-resistant capabilities,[13–15] further necessitating the ability to examine interactions between small molecules (*i.e.* drug molecules) and living cells. As such, how small molecules adsorb and subsequently traverse this complex boundary is a facet of the scientific community that offers insight into drug development and understanding antibiotic mechanisms of actions.[16–23]

Thus far, a majority of experiments capturing these phenomena are conducted on model systems although the compositions of the most commonly studied mimetic membranes differ drastically from that of infectious Gram-positive bacteria. For instance, fluidity in model systems is mostly mediated by various degrees of saturation in the fatty acid tails and cholesterol content, while for bacteria, fluidity is primarily determined by the abundance of branched-chain fatty acids instead.[24,25] The highly negatively charged bacterial membrane is an additional factor that makes mimicking this environment a difficult task. Although

there has been progress in addressing these discrepancies, model systems are still overall limited, particularly for Gram-positive bacteria.[26–31] Due to the prevalence of Gram-positive bacteria in life-threatening infections,[32,33] it is of paramount importance to understand how small molecules navigate the living cell membrane terrain. LogP values, a measure of a molecule's partitioning ability between hydrophobic and hydrophilic environments, is one of the primary considerations for predicting membrane permeation in current methods of drug design and alteration. Specifically, molecules with more positive computed LogP (cLogP) values are more lipophilic and thus more prone to membrane penetration up to the threshold of 5 after which reduced penetration is expected.[34] However, this approach is not always reliable, and new rules governing this behavior are needed.[3] Here, we examine how tunable parameters of small molecules, such as charge and lipophilicity, alter their adsorption and movement within the living membranes of Gram-positive bacteria, *S. aureus* and *B. subtilis* by leveraging the surface specificity of second harmonic generation (SHG).

The membrane space of living bacteria is historically difficult to probe due to, for example, a typical *S. aureus* cell spanning $\sim$1 μm in diameter and the lipid bilayer averaging $\sim$5 nm in thickness.[35,36] Exploring intrinsic dynamics in real-time at this spatial scale is difficult due to traditional techniques being either destructive to the living specimens or lacking resolution and specificity. While electron microscopies have capabilities to resolve structures on these spatial length scales, sample preparation requires cells suspended in time.[37–42] Additionally, separation and subsequent mass spectrometry techniques are also limited by their destructive nature.[43–48] While not generally detrimental to biological samples, traditional light-based microscopies, such as one-photon fluorescence modalities, are limited by the diffraction limit of light.[4,49–52]

Aside from the technical limitations experimental techniques pose, living cells are impressively complex, and thus, oftentimes computational methods and, as mentioned above, mimetic membranes, such as planar or vesicular lipid bilayers, are employed to explore fundamental properties such as transport through the membrane.[30] Model membranes serve as

a simplistic view of an otherwise complicated space and have offered an abundance of fundamental insight into small molecule passive diffusion. Of special interest is a membrane's ability to migrate cargo from one leaflet of the lipid bilayer to the other (*i.e.*, flip-flop) as this movement is responsible for the diffusion of small molecules, incorporating newly synthesized phospholipids from the intracellular environment to the outer leaflet, and maintaining lipid asymmetry.[53] This is also often seen as the rate-limiting step in permeation making it a crucial parameter in assessing antibiotic penetration.[54] As such, much attention has been devoted to understanding which small molecule structural parameters impact the molecule's ability to flip-flop. There is a large body of literature proposing that contributions from the polar/charged headgroup and the hydrophobic tail regions have significant impacts on the rate at which flip-flop occurs. For instance, many have shown that the charged nature of fatty acids and phospholipid headgroups predominantly impact the rate of flip-flop,[55,56] while others have shown that their hydrophobic tail portion may play a larger role than initially thought.[57,58] Others have shown that both should be regarded as having considerable impacts on their translocation capabilities.[59,60] Among this debate, other differences between classes of molecules have also been linked to dictating translocation rate. For instance, Regev, *et al.* have shown with a series of drug molecules that there is no correlation between their lipophilicity and their flip-flop kinetics;[61] Rog, *et al.* and Parisio, *et al.* attributed changes in sterol polarities to their flip-flop discrepancies;[62,63] and lastly, Rokiskaya, *et al.* describe conflicting results owing to a small ions ability to flip-flop in correlation with their size and hydrophobicity.[64,65] However, this large range of results suggests that the impact of these molecular parameters are highly influenced by the composition of the membrane under investigation.[58,66,67]

While there has been tremendous progress toward understanding how small-molecule structure influences permeation and flip-flop, there remains a necessity to employ techniques that are able to directly monitor the impacts of these parameters on living cells as their membranes are expected to be far more complex in structure and function than that of model

systems. Gram-positive bacteria, such as *S. aureus*, serve as ideal bridges between studies on living and model systems. As living cells, they have a complex membrane composition as well as direct relevance for human health, but they also contain only a single plasma membrane with a size and uniform curvature reminiscent of model vesicles. As Gram-positive bacteria, however, the lipid composition of their membranes varies significantly from many of the model systems typically employed, specifically the headgroup species, lack of cholesterol, and the presence of branched fatty acid chains in contrast to the unsaturated fatty acid chains most prevalent in the previously mentioned models.[68] Therefore, here, we use SHG, a surface-specific nonlinear optical technique, to examine differences between structural variants of small molecules and their interactions with living cells.

SHG relies on the interaction of two photons of the same energy with a noncentrosymmetric medium to generate a single photon of twice the incident photon energy.[69] Because of the symmetry requirement for this process, interfaces and surfaces make ideal candidates to study with SHG as symmetry is inherently broken. SHG has previously been employed in many experiments to quantify the adsorption and transport kinetics of small molecules across the membranes of model systems,[70–80] living eukaryotic cells,[81–85] and live bacteria.[9,86–96] As such, we have previously illustrated the membrane adsorption characteristics and subsequent behavior of the styryl dye molecules FM 2-10 and FM 4-64, within *Enterococcus faecalis* and *S. aureus* membranes with SHG and two-photon fluorescence.[9] In regards to *S. aureus*, Miller *et al.* determined that the smaller, less lipophilic FM 2-10 molecule had a significantly weaker affinity for the membrane environment, thus following predictions posed by Overton's Rule.[97,98] However, the more surprising result was how the conjugation length altered their dynamics within the membrane over time. It was observed that the more highly conjugated FM 4-64 molecule had a greater propensity to experience flip-flop while FM 2-10 had a more complex behavior associated with either aggregation or movement into more rigidly organized membrane domains.[9] This study further demonstrated the feasibility of using SHG to evaluate molecule dynamics in living Gram-positive membranes. As drug

molecules exhibit drastically different effects on their target cells from minuscule alterations in their structure,[99,100] it is imperative to understand how the individual moieties, aside from conjugation length, impact the independent steps of permeation, including flip-flop. There exists multiple styryl dye molecules, beyond these two, that differ in their charged headgroups, conjugation length, and branching in their tail region. By expanding our studies to include a wider range of these molecules and other cell types, we can begin to tease apart the factors with the most significant influence on the interplay between the molecules and membranes.

Styryl dyes are popular membrane probes as they exhibit distinctive fluorescence signatures when bound in lipophilic environments as opposed to free molecules in solution.[101,102] Additionally, their non-symmetric induced dipoles make them 'SHG-active' in that they can produce prominent second harmonic signals dependent on how their individual dipoles are arranged along the membrane surface. The second harmonic signal produced is sensitive to how the molecules are arranged relative to one another and in response to their immediate environment, as explained schematically and mathematically below in Figure 1 and Equations 1 and 2, respectively.

The SHG signal (I_{SHG}) resulting from the alignement of molecules at an interface is directly proportional to the product of the two incoming electric fields (E_ω) and the effective second-order nonlinear susceptibility term ($\chi^{(2)}_{eff}$) as depicted in Equation (1).

$$I_{SHG} = \mid E_{SHG} \mid^2 = \mid \chi^{(2)}_{eff} E_\omega E_\omega \mid^2 \tag{1}$$

$\chi^{(2)}_{eff}$ is a tensor element that describes the symmetry dependence of the resulting signal. Assuming the electric field of the incoming light being applied to a sample stays constant for the duration of an experiment, it can also provide insight into the source of change in the intensity of an SHG signal over time by considering its two constituent terms:

$$\chi^{(2)}_{eff} \propto N_s \langle \beta \rangle \tag{2}$$

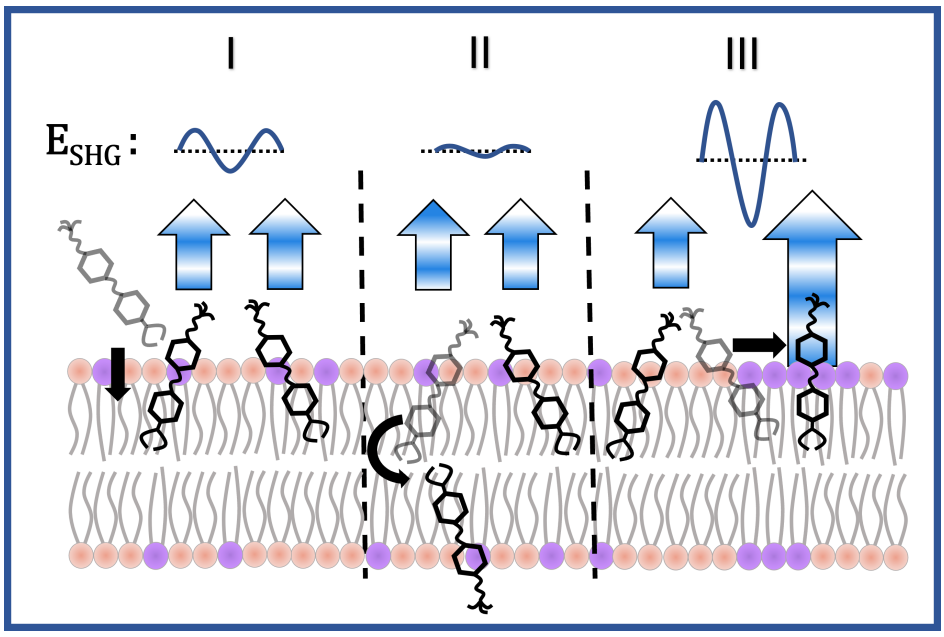

Figure 1: Cartoon schematic of styryl dye molecules interacting with a lipid bilayer and the resulting SHG signals (E_{SHG}). After adsorption to the membrane, (I) dye molecules produce an initial SHG signal. The molecules can then either (II) flip-flop to produce destructive SHG signals, or (III) migrate to a more rigid environment that enhances the overall orientationally averaged hyperpolarizability, producing a greater intensity SHG response.

As seen in Equation (2), the value of $\chi^{(2)}_{eff}$, and therefore the resulting SHG intensity, can be described by 1) the relative population of the probe molecules in the membrane (N_s) and 2) the orientational average of the hyperpolarizability ($\langle\beta\rangle$). N_s is simply determined by how many molecules are being illuminated in the noncentrosymmetric space of the bacterial surface and can vary depending on the number of surface sites available and the probe molecule concentration. In the second term, the hyperpolarizability alone (β) refers to the oscillatory strength of the light-induced dipole in response to the molecule's chemical environment (i.e. presence of ions and/or solvent identity), whereas $\langle\beta\rangle$ describes the orientational average of the overall arrangement of these dipoles. Figure 1 illustrates how the latter term can alter the ensuing signal. In each case displayed, the number of probe molecules stays constant, but the orientation of them varies. In panel I, two molecules are inserted into the outer leaflet of the example lipid bilayer. Assuming the location of these probe molecules is in a fluid-like region of the membrane, the probes will insert with a large degree of variability in

their angular orientation with respect to each other, and thus a less-than-perfect constructive interference of their second harmonic signals. After initial adsorption into the outer leaflet, possible fates of the molecules are shown in the successive panels. In panel II, it is illustrated how when one of the molecules present in the outer leaflet flip-flops into the inner leaflet, the orientation of each molecule arranges in an anti-parallel fashion producing opposite phases, and thus, destructive interference lowering the SHG intensity. Lastly, as illustrated in panel III, the probe molecules could instead migrate to a more rigid environment in the membrane space. The rigidified lipids surrounding the membrane probe reduce the variability in the molecules' angular orientation promoting a higher degree of alignment with one another. This phenomenon significantly increases the $\langle\beta\rangle$ term and the resulting SHG intensity.

Herein, we perform a series of experiments to answer the following posed questions: 1) How do the size and shape of the hydrophobic moieties impact the molecules' behavior in the membrane of a living cell? 2) Does the headgroup identity have a significant role in these dynamics? and, 3) What role does membrane composition impart in the context of living cells? The answers to these questions can inform on what aspects of small molecule structure may be tuned to alter their overall permeation capabilities and how well model systems capture these disparities. As such, we examine the structural parameters of headgroup identity, length of the conjugated region, and the length of the branched tails on molecules FM 2-10, FM 4-64, FM 1-43 and 4-Di-2-ASP (Figure 2). The latter two parameters allow us to differentiate between the impacts of overall hydrophobicity versus the shape of the hydrophobic region. Additionally, we examine the impact of the membrane composition by showing differences in molecule dynamics in the membranes of *S. aureus* and *B. subtilis*.

We employ SHG in two ways: first to quantify the adsorption of the aforementioned molecules onto living bacterial cell membranes with adsorption isotherm experiments, and second, to monitor the movement of the molecules with time-resolved SHG measurements. We determine that branching in the tail of the probe molecules has minimal impact on the initial interactions but drastically impacts flip-flop once inserted into the membrane com-

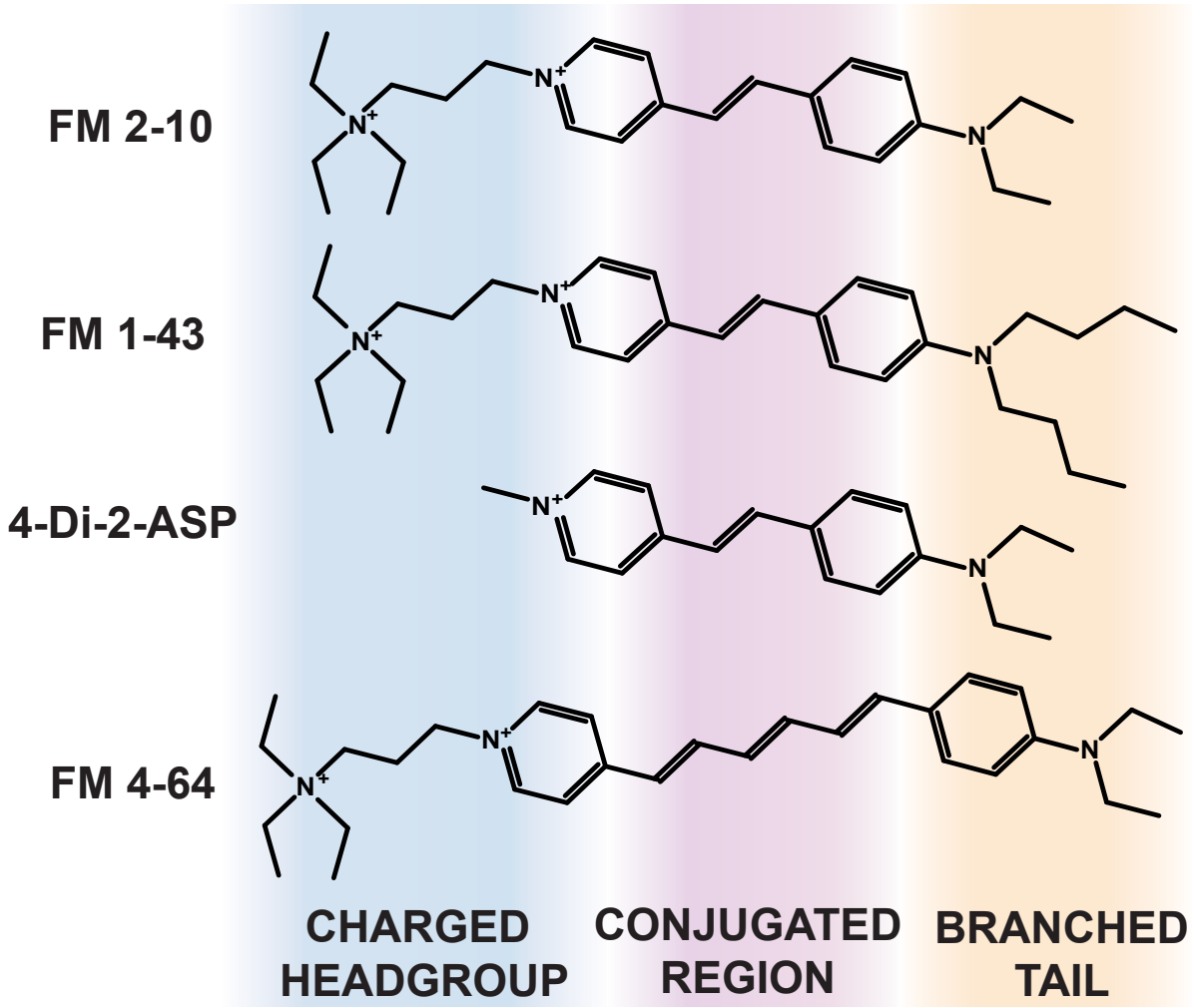

Figure 2: Structures of membrane probes FM 2-10, FM 1-43, 4-Di-2-ASP, and FM 4-64. Chemical structures of the probe molecules with colored shaded background regions indicating the charged headgroup (blue), conjugated region (purple) and the branched tail (orange).

pared to a molecule with its hydrophobic tendencies localized in a straight conjugated chain. Conversely, we show that the headgroup identity plays a small role in membrane affinity and, for *S. aureus*, little difference in dynamics over time, in direct opposition to model systems. However, by performing similar experiments with *B. subtilis*, we determine that the membrane composition is a crucial determinant in the dynamics imparted by headgroup identity.

Results and Discussion

Impacts of Molecule Structure

Tail Branching and Conjugation Length

We start our analyses by considering the hydrophobic moieties of the probe molecules, namely the conjugated regions and branched tails highlighted by the purple and orange regions in Figure 2. First, we will examine how this region influences the affinity of the probe molecules to the membrane environment. This is quantified by fitting the SHG responses to increasing probe molecule concentration to a Langmuir adsorption model (see Materials and Methods). In doing so, the dissociation constant (K_d) for each molecule can be extracted. The K_d values are indicative of the fraction of the rate molecules are dissipating (k_{off}) from to the rate they are adsorbing to the lipid bilayer (k_{on}) which is representative of the concentration of molecules required to inhabit 50% of the available binding sites on the membrane. As such, the lower the K_d value is, the higher affinity the probe molecule has for the membrane. We have previously assessed the adsorption behavior of the probes FM 4-64 and FM 2-10 (K_d values shown in Table 1).[9] As such, we have shown that the increased lipophilic nature of FM 4-64 resulted in an increased affinity for the membrane environment. Here, we extend our studies to consider how the shape of the branched portion may impact initial adsorption. Specifically, between FM 4-64 and FM 1-43 (Fig. 3b), there is no significant difference

between their affinities to the membrane, despite a relatively large difference in their cLogP values, -1.6 vs. -0.29, as determined by ChemDraw software and listed in Table 1. These two molecules are expected to reside in the same depth as their hydrophobic moieties are similar in length. However, their hydrophobic moieties are distributed differently where FM 4-64 has a longer straight conjugated chain and FM 1-43 has longer saturated carbon chains extended from the tail. We expect this structural difference between FM 4-64 and FM 1-43 will allow for differing lateral occupation. It can be noted, however, that this difference in lateral occupation does not lead to any difference in anchoring within the membrane as the k_{off} values between these molecules are presumably comparable given the similarities in their K_d values. As such, the width of the molecule seems to have minimal effects on the overall adsorption to the membrane space of *S. aureus*. Therefore, the more notable feature giving rise to a strong affinity to the membrane is the overall hydrophobic moiety lengths of the molecule regardless of whether this property lies in the branched tail or the conjugated chain.

Table 1: Dissociation constants (K_d) and cLogP values[a] for each membrane probe for *S. aureus* and *B. subtilis* extracted from SHG adsorption isotherms fit to the Langmuir adsorption model.[b]

Membrane Probe	***S. aureus*** $\mathbf{K}_d(\mu\mathbf{M})$	***B. subtilis*** $\mathbf{K}_d(\mu\mathbf{M})$	**cLogP**
FM 4-64	14.5 ± 5[c]	-	-1.6
FM 1-43	9.0 ± 1.6	-	-0.29
FM 2-10	280 ± 33[c]	72.1 ± 21	-2.4
4-Di-2-ASP	152 ± 40	56.7 ± 13	-0.28

[a] Values were obtained from ChemDraw software.
[b]Error is displayed as standard error to the fit of the model, $n = 3$ for each probe.
[c]K_d values reported in [10]

While increasing both the length of the branched tail and the conjugated region resulted in similarly increased affinities for the membranes, the individual contributions to the molecule's architecture show significant time dynamic discrepancies. First, we will discuss the impact of increasing the length of the conjugated region, while the rest of the

molecule remains the same. To do so, we will directly compare the behavior observed in the time-dependent trials of FM 2-10 and FM 4-64, as shown in Figure 4b. We have previously reported how increasing only the conjugation length changes the dynamics of the small molecules within the membrane over time.[9] Briefly, the less lipophilic molecule (see cLogP values in Table 1), FM 2-10, shows an increase in SHG signal as is also shown in this report. In contrast, the FM 4-64 probe experiences a decrease in SHG signal over time indicative of flip-flop. We consequently concluded that increased conjugation, and thus increased lipophilicity, results in flip-flop.

To address the other crucial facet of the hydrophobic nature of the molecules, the branched tail, we compare the overall shape of this region between FM 4-64 and FM 1-43. As stated previously, both FM 4-64 and FM 1-43 have comparable adsorption affinities for the *S. aureus* membrane. However, the structural differences between the two molecules result in varying behaviors in the membrane space over time. Both molecules experience flip-flop indicated by a relative decrease in SHG signal over time but, as seen in Figure 4c, while FM 4-64 slowly decreases until it reaches approximately 50% of its maximum intensity after the two-hour duration, the FM 1-43 molecules flip-flop more rapidly, reaching it's lowest intensity within 30 minutes but then slowly rises in signal for the remainder of the experiment which may indicate aggregates forming in one or both bilayer leaflets or the eventual migration of molecules to more rigid environments, as depicted in Figure 1. These discrepancies can be explained by the increased length of the *branched region* in the tail of the FM 1-43 probe in comparison to the two-carbon chains of FM 4-64. As alluded to above, FM 1-43 occupies a larger lateral site than would be expected for the straighter FM 4-64 molecules when adsorbed to the membrane due to the increased width in the tail region of the FM 1-43 molecules. By requiring more lateral space in the membrane, the FM 1-43 molecules can be expected to create an immediate area of increased fluidity which may provide the space to facilitate flip-flop. Alternatively, this difference in lateral occupation may vary the probe molecule's affinity for certain portions of the membrane in which FM 1-43 is

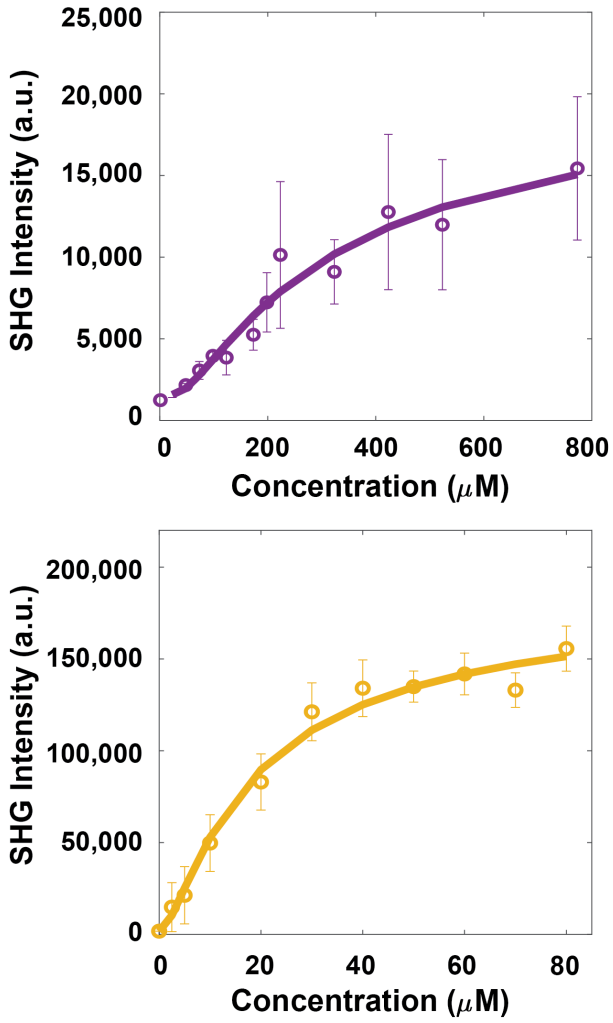

Figure 3: SHG adsorption isotherms of 4-Di-2-ASP (top) and FM 1-43 (bottom) with *S. aureus* living cells. For each probe, $n = 3$. Circles ($\circ$) represent the averages of the individual trials while the solid lines (—) are the fits from the Langmuir model. Error bars are representative of standard deviations. K_d values are shown in Table 1

attracted to more fluid-like regions that were already present in the membrane. While the studies monitoring impacts from the hydrophobic tails mentioned above increase the length, here, we are examining a modification to the lateral structure in addition to the length.

It is interesting to acknowledge that while FM 1-43 molecules primarily flip-flop in the membrane space of *S. aureus*, alternate mechanisms begin to arise soon thereafter - a transpiration not previously considered a possibility as it is not commonly reported in model systems. This implies that the dynamic landscape of the bacterial membrane is mediating additional organizational forces. Further, it seems that this phenomenon is highly dependent on the probe molecule's structure as a rise is not seen during the same time period for FM 4-64. The results from this experiment further demonstrate the necessity to monitor flip-flop and potential events occurring afterward in living cell membranes.

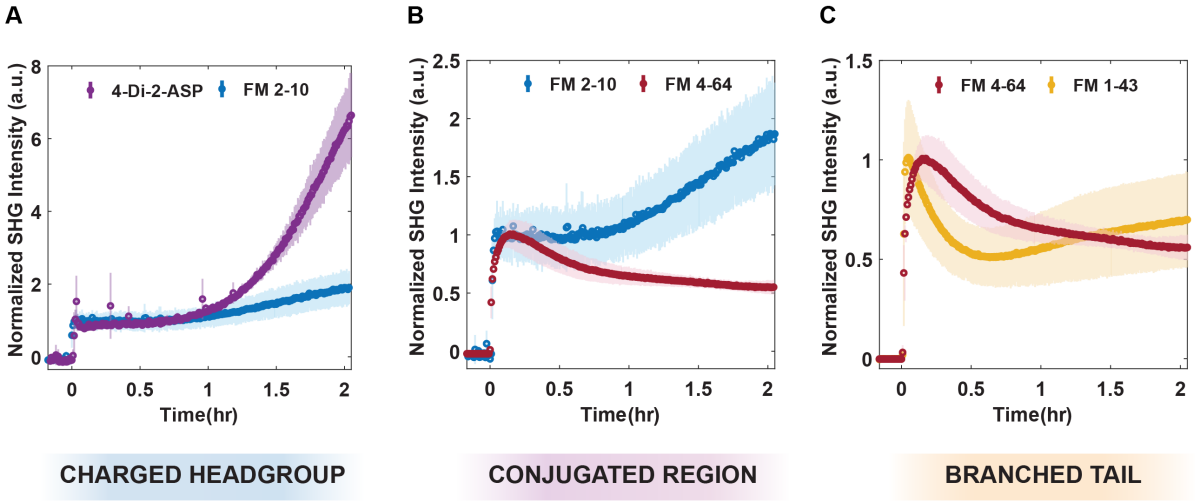

Figure 4: 16 μM membrane probe time-dependent SHG trials with *S. aureus* cells. (A) shows how headgroup identity impacts membrane dynamics (4-Di-2-ASP versus FM 2-10), (B) compares FM 4-64 and FM 2-10 to show differences arising from conjugation length, and (C) portrays similar lipophilic lengths of FM 1-43 and FM 4-64 having comparable SHG responses. For each membrane probe, $n = 3$ and shaded regions represent the standard deviation between the individual trials.

Impact of Probe Headgroup Charge/Size

The headgroup of membrane-residing small molecules has been hypothesized to be a crucial ingredient when attempting to promote flip-flop dynamics.[55,56,62,63] By comparing molecules FM 2-10 and 4-Di-2-ASP (Fig. 2), we can directly assess how the contributions arising from the headgroup region impacts initial adsorption and subsequent membrane dynamics. The K_d values observed for probes FM 2-10 and 4-Di-2-ASP are both significantly greater than those witnessed for molecules FM 4-64 and FM 1-43, discussed above. Moreover, it can be seen that the reduced headgroup charge from +2 on FM 2-10 to that of +1 on 4-Di-2-ASP results in a smaller K_d value signifying the singly-charged molecule has a greater affinity for the membrane. Aside from differences in charge, FM 2-10 has a bulkier substituent in the headgroup so sterics may also be involved in the differences seen between FM 2-10 and 4-Di-2-ASP adsorption. Further, the adsorption discrepancies between FM 2-10 and FM 1-43/FM 4-64 are expected as FM 2-10 is significantly less lipophilic than both FM 1-43 and FM 4-64. However, 4-Di-2-ASP is the most lipophilic molecule of the four examined here, as determined by their cLogP values (Table 1. These results show that the cLogP values are not always reliable indicators of membrane adsorption.

The time-dependent experiments performed with FM 2-10 and 4-Di-2-ASP interacting with *S. aureus* show that these two molecules exhibit the same overall dynamics, although to different extents. As can be seen in Figure 4a, both show a relatively static initial signal with an overall increase in SHG over the two-hour time period. We have previously considered both cell growth and increased probe population (*i.e.* components responsible for changes in N_s, Eq. 2) in the membrane space as contributing factors to this rise in signal.[9] However, we have shown that the cells are restricted in their growth by the temperature at which these experiments are conducted and the two-photon fluorescence signal remained fairly static throughout the course of the experiments.[9] As such, as seen by Equation 2, this leaves the only contribution to an increase in SHG to be due to a change in the $\langle\beta\rangle$ term. As discussed above, the increase in this term could arise from the probe molecules associating

with a change in solvent identity or neighboring lipids, aggregating in the membrane space, or moving to more rigid environments.

While both rise in signal, 4-Di-2-ASP appears to have a more significant rise in comparison to FM 2-10. In fact, while the overall SHG intensity increases by the two-hour mark for both membrane probes, the final SHG intensities rise more than a factor of 7 and 2 for 4-Di-2-ASP and FM 2-10, respectively. As discussed above, the charge, steric characteristics, or a combination of both, may be the cause of this behavior. We hypothesize that the quicker rate and larger signal may be due to the reduced charge and size of 4-Di-2-ASP causing less repulsive forces between one another while embedded in the membrane resulting in more favorable lateral migration throughout the membrane. The decrease in size may enable a tighter packing of probe molecules in the membrane which could cause a large rise in SHG signal, as observed here.[103,104] More importantly, while others have seen that decreasing the sterics and altering the charge of the headgroup may lead to an increased rate of flip-flop,[54,65] this phenomenon is not observed here. In fact, it appears that 4-Di-2-ASP has a greater aversion to flip-flop than FM 2-10 which is in opposition to what is commonly reported for model systems. Additionally, as for 4-Di-2-ASP, in the presence of one particular type of model vesicles, it was shown that the molecules readily flip from one leaflet into the other, with no indications of aggregation or organization.[79] The discontinuities described here between our experiments and those performed on model systems further illustrate the necessity for future experiments to supplement the repertoire of molecules with varying headgroup charge and/or size in the context of living cells.

Impacts of Membrane Composition

It is ubiquitously agreed upon that the bilayer lipid composition influences molecule-membrane dynamics among the mimetic membrane community.[58,66,67] However, the extent of this factor has yet to be fully explored in living bacterial cells. We have shown here that the membrane identity plays a crucial role in the dynamics displayed by a small molecule. As alluded

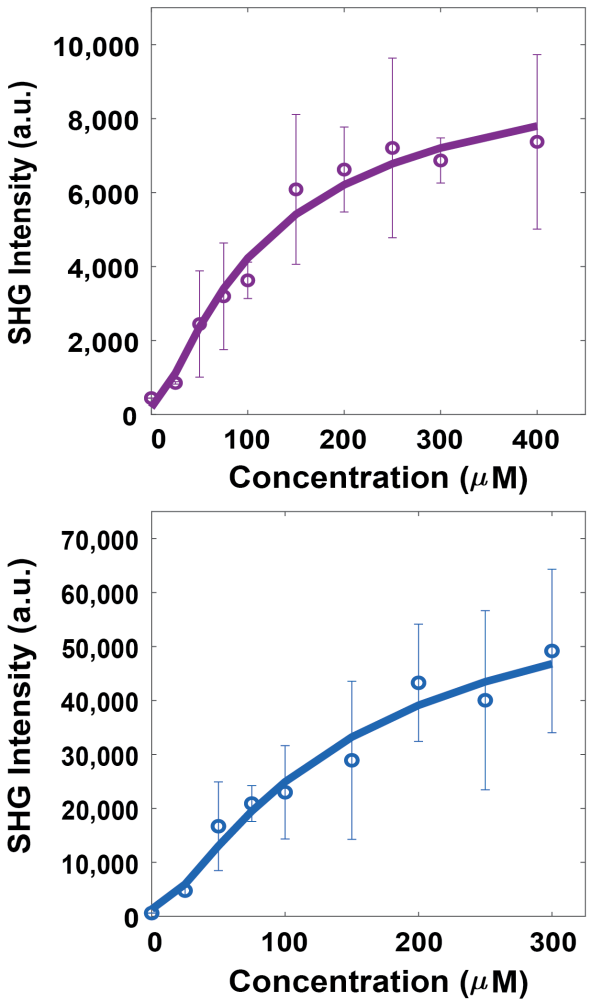

Figure 5: SHG adsorption isotherms of 4-Di-2-ASP (top) and FM 2-10 (bottom) with *B. subtilis* living cells. For each probe, $n = 3$. Circles ($\circ$) represent the averages of the individual trials while the solid lines (—) are the fits from the Langmuir model. Error bars are representative of standard deviations. K_d values are shown in Table 1

to above, *B. subtilis* is another Gram-positive bacterium that differs from *S. aureus* by its shape, protein population and lipid headgroup and tail identities. Our purpose for studying this cell species was to address the generality of the claims gathered from our experiments with the FM dyes presented here and *S. aureus*. To do so, we focused on revisiting the apparent minimal role of the headgroup identity on adsorption and dynamics over time.

As can be seen in Figure 5 and Table 1, FM 2-10 and 4-Di-2-ASP have considerable differences in their affinity to *B. subtilis* compared to *S. aureus*. Although the trend remains the same - the smaller, less bulky headgroup substituent results in a greater affinity to the cell species - the magnitude of the molecules' affinity is greater for *B. subtilis*. Specifically, FM 2-10 has an affinity for the *B. subtilis* membrane $\sim$4 times greater than that for *S. aureus*. Similarly, the K_d of 4-Di-2-ASP is $\sim$3 times larger for *S. aureus* than *B. subtilis*. However, the results from the time-dependent trials reveal the two probe molecules demonstrate starkly different dynamics in *B. subtilis*. Whereas FM 2-10 had an immediate rise due to adsorption and a subsequent slow increase over the duration of the experiment in *S. aureus*, for *B. subtilis*, the second rise for the probe molecule, associated with membrane organization, is $\sim$6 times faster. Soon thereafter, the signal in *B. subtilis* decays slightly and remains fairly constant for the duration of the experiment. However, 4-Di-2-ASP did not share this trend at longer times. Despite 4-Di-2-ASP displaying a large propensity to remain in the outer leaflet of *S. aureus*, the exact opposite occurs when this molecule interacts with *B. subtilis*. After the initial interaction, a slight rise is detected similarly to FM 2-10 with *B. subtilis*. Following this increase in signal, instead of a drastic rise over time as seen with *S. aureus*, 4-Di-2-ASP in the *B. subtilis* membrane environment exhibits flip-flop at a rate congruent to FM 1-43 with *S. aureus*.

This discrepancy in membrane dynamics most likely arises due to differences in membrane composition and organization between these two bacteria. A recent study on model systems has proposed that membrane thickness is one of the leading parameters controlling small molecule permeation.[105] Based on electron microscopy experiments, the membrane

thickness of *S. aureus* is 5.4±0.4 nm[36] while the *B. subtilis* plasma membrane was found to be thicker at 6.6±0.8 nm.[106] Given that more flip-flop is observed in our *B. subtilis* experiment, membrane thickness is not expected to be the dominant contributor. Both *B. subtilis* and *S. aureus* have been shown to possess membrane structural heterogeneity, most commonly referred to as regions of increased fluidity (RIFs) or functional membrane microdomains (FMMs), respectively, which are thought to play roles in passive diffusion of small molecules.[105,107,108] Fluidity in the membranes of both species is controlled by the ratio of branched-chain fatty acids (BCFAs) of the lipids. The percentage of BCFAs in the membranes of these bacteria is starkly different: ∼50 of the lipids in the *S. aureus* plasma membrane contain BCFAs[109] while in *B. subtilis* this is over 90%.[26,110] This disparity in BCFA amount, and thus membrane composition, results in differing overall membrane fluidity and organizational forces. The more fluid membrane corroborates what is commonly seen in the literature where a smaller headgroup results in a quicker flip-flop rate, and thus a greater propensity to do so.[65] However, these results show that this generalized statement cannot be applied to all systems, especially complex and dynamic living bacterial membrane systems.

Conclusions

In summary, we have shown through the interface specificity of second harmonic generation that the fate of small molecules interacting with the membrane of living *S. aureus* can be tuned through specific structural changes. Moreover, we have shown that the dynamics of these small molecules cannot be generalized for all membrane systems, or even the seemingly similar Gram-positive bacterial membranes, by illustrating that dynamics of small molecules are also dependent on the membrane composition. Through adsorption kinetic studies, we have found that the major factor contributing to initial interactions is reliant on the length of the hydrophobic region of the molecule, no matter whether that length resides in the

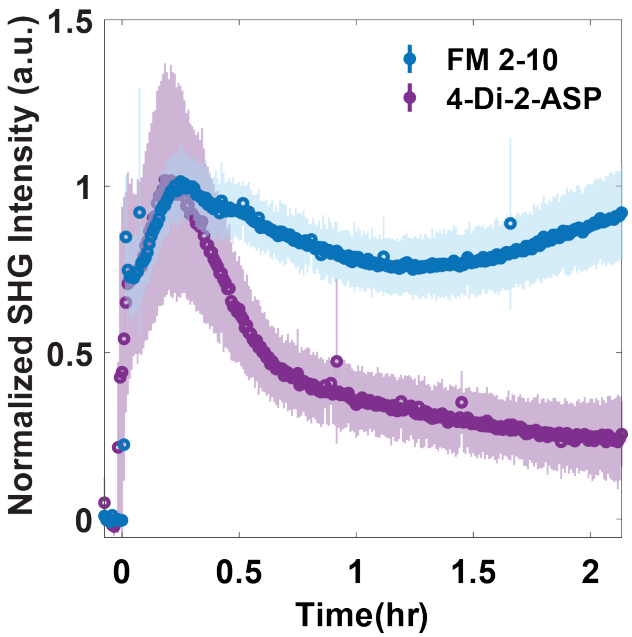

Figure 6: 16 μM 4-Di-2-ASP and FM 2-10 time-dependent normalized SHG trials with *B. subtilis* cells. For each membrane probe, $n = 3$ and shaded regions represent the standard deviation between the individual trials.

conjugated chained region or the branched tail of the styryl dyes presented here. However, these results do not always trend along with apparent LogP values. To a smaller degree, we have also shown that a smaller charge and size in the headgroup region of the small molecule interacting with the phospholipid headgroups of the lipid bilayer are associated with stronger adsorption to the outer leaflet for both species investigated. These initial adsorption experiments support what has been shown in the literature regarding how the structure of a small molecule impacts binding to the membrane space of model systems despite models, eukaryotic cells, and bacteria displaying differences in phospholipid headgroup distributions.[68]

The time-dependent experiments presented here provide new insight as to what parameters on small molecules result in flip-flop versus the molecules undergoing predominate organization in the outer leaflet. For *S. aureus*, smaller molecules, FM 2-10 and 4-Di-2-ASP, show a propensity toward the latter while larger, more lipophilic molecules exhibit flip-flop. More specifically, increasing the length of the branched tail, and more so the width of the

tail, promotes the most rapid flip-flop observed for the molecules examined. However, as exhibited by FM 1-43, the small molecules may be subjected to additional organization by living cell membranes after flip-flop has occurred. This finding is significant in that we explicitly show lateral contributions should be considered when assessing flip-flop dynamics as well as the events taking place afterward. As for *B. subtilis*, there was a greater impact from the headgroup identity with the singly charged 4-Di-2-ASP molecule exhibiting a large degree of flip-flop, demonstrating how the membrane composition can alter these dynamics. These results are not only important considerations for designing drugs that will successfully penetrate into bacterial cells but can also be exploited to target specific cell species.

Materials and Methods

Bacterial Strains and Dye Solutions

S. aureus (ATCC 27217) and *B. subtilis* 168 were the bacteria used in the experiments outlined above. Cells were prepared similarly to what we have done previously.[9] *S. aureus* and *B. subtilis* cells were incubated overnight on brain-heart infusion (BHI)(Sigma-Aldrich, St. Louis, MO) and Luria-Bertani Broth (LB)(Sigma-Aldrich, St. Louis, MO) agar plates , respectively. Single colonies were then inoculated into liquid BHI or LB with a 1:5 media-to-head space ratio. Flasks of *S. aureus* and *B. subtilis* were grown anaerobically and aerobically at 250 RPM, respectively, overnight at 37°C until cells reached stationary phase and then transferred to fresh media to an optical density at 600 nm (OD_{600}) of ∼0.01 and grown until the OD_{600} reached ∼0.2. OD's were measured using an ultraviolet-visible spectrophotometer (SHIMADZU UV-2600; Shimadzu, Columbia, MD). Once the appropriate OD was reached, the cells were filtered using a 0.22-micron cellulose nitrate vacuum filter with phosphate buffered saline solution and subsequently resuspended into BHI or LB supplemented with 2% EC-OxyRase to an OD_{600} of ∼0.2. All cell samples were prepared immediately before beginning each trial.

For each dye, 0.4, 0.8 and 1.6 mM stock solutions were prepared in 0.2 micron filter-sterilized 80:20 MilliQ water (Sigma-Aldrich, Burlington, MA; 18.2 MΩ · cm) to dimethyl sulfoxide (DMSO) (Thermo Fisher Scientific, Suwanee, GA). FM 2-10 (SynaptoGreen C2), FM 1-43 (SynaptoGreen C4), and FM 4-64 (SynaptoRed C2) were purchased from Biotium (Fremont, CA). 4-Di-2-ASP (4-di-2-asp) was purchased from Sigma-Aldrich. All probe molecules were used as received.

SHG Instrument and Flow Cell Passivation

A home-built SHG spectroscopy instrument was used in the adsorption isotherms and time-dependent experiments, details of which have been previously described elsewhere.[9,86] Briefly,

laser pulses from an 80 MHz MaiTai Ti:Sapphire oscillator (Spectra Physics, Santa Clara, CA) compressed to approximately 95 fs were directed through a power attenuator comprised of a half-wave plate and polarizing beam splitting cube and then sent towards the sample housed in a 2 mm path length quartz flow cell (Starna Cells, Atascadero, CA). After traversing through the sample, the forward propagating signal was collected through a series of lenses followed by a fiber and sent to a photomultiplier tube (Hamamatsu, Bridgewater, NJ) and filters to collect SHG responses. A 450 nm long pass filter (Edmund Optics, Barrington, NJ) was placed before the sample to ensure the second harmonic frequency being detected was produced from the sample itself and not any previous optics. A 725 nm short pass filter (Edmund Optics) was placed directly before the optical fiber to omit the fundamental wavelength. For all cases, a 400/10 nm bandpass filter (Edmund Optics) was used directly before the respective PMT to obtain the SHG response. Additionally, malachite green/polystyrene beads power studies were carried out both before and after data collection to ensure instrument stability.[111] All data was collected using LabView and analyzed with MATLAB using in-house codes.

To ensure no cell or protein adsorption onto the sample housing, the quartz flow cell was passivated 30 minutes before each individual isotherm and time-dependent trial using a bovine serum albumin (BSA)(Sigma-Aldrich)/1% glutaraldehyde (Thermo Fisher Scientific) cross-linking procedure.[112] Briefly, 1 M hydrochloric acid was introduced to the flow cell for $\sim$30 minutes and then flushed with 50 mL of sterile MilliQ deionized water. Cold ($\sim$ 4°C) 10 mM Tris buffer (pH adjusted to $\sim$7.4) (Sigma-Aldrich) was then rinsed through to prepare for the BSA solution. BSA was prepared immediately before introduction to the flow cell with Tris buffer to a final concentration of 50 mM and then filter sterilized with a 0.22 micron PES filter. BSA was incubated in the flow cell for 10 minutes and then followed with a 10 minute incubation period of a 1% glutaraldehyde solution prepared with Tris. Lastly, Tris was flushed through once more. Air was pushed through the flow cell followed by a 1 mL aliquot of prepared cells that was then discarded.

Adsorption Isotherms

For the SHG adsorption isotherm experiments, 990 μL of cells suspended in BHI and 2% OxyRase were aliquoted into sterile micro-centrifuge tubes. Stock solutions of each dye were made in a filter-sterilized solution of 80:20 MilliQ water:DMSO. A serial dilution of the dye solutions were prepared into separate sterile micro-centrifuge tubes. To prepare the sample, the dye was introduced into the aliquot of cells for a final DMSO concentration of 0.2% and then transferred to the quartz flow chamber. Data were acquired immediately after sample preparation. Cells were exposed to 350 mW of light for a total of 1 s with the signals being recorded every 25 ms. A Langmuir adsorption isotherm model was then fitted to the average of 3 trials to obtain the dissociation constant (K_d) of each dye:

$$\theta = \frac{\frac{[c]}{K_d}}{1 + \frac{[c]}{K_d}} \tag{3}$$

where θ is the number of available binding sites and [c] is the concentration of available probe molecules.[9,86,113,114]

Time-dependent Experiments

A home-built gravity flow apparatus with autoclave-sterilized tubing was used in the time-dependent experiments. In a sterile media bottle, 7 mL of cells in BHI/OxyRase were flowed cyclically through the apparatus at a rate of $\sim$7 mL/min. Signal was recorded every 25 ms for a total of 8000 s with 70 μL of dye solution being introduced to the initial reservoir of cells at 600 s for a final DMSO concentration of 0.2%. Power was reduced to 35 mW for these experiments due to the extended period of data collection.

Acknowledgement

The authors thank the National Institute of General Medical Sciences of the National Institutes of Health under award number R35GM142928 and the National Science Foundation REU fellowship under award number NSF-CHE-1852160 for support.

References

(1) Strahl, H.; Errington, J. Bacterial Membranes: Structure, Domains, and Function. *Annual Review of Microbiology* **2017**, *71*, 519–538.

(2) Willdigg, J. R.; Helmann, J. D. Mini Review: Bacterial Membrane Composition and Its Modulation in Response to Stress. *Frontiers in Molecular Biosciences* **2021**, *8*.

(3) Lewis, K. Platforms for Antibiotic Discovery. *Nat Rev Drug Discov* **2013**, *12*, 371–387.

(4) Bach, J. N.; Bramkamp, M. Flotillins Functionally Organize the Bacterial Membrane. *Molecular Microbiology* **2013**, *88*, 1205–1217.

(5) García-Fernández, E.; Koch, G.; Wagner, R. M.; Fekete, A.; Stengel, S. T.; Schneider, J.; Mielich-Süss, B.; Geibel, S.; Markert, S. M.; Stigloher, C.; Lopez, D. Membrane Microdomain Disassembly Inhibits MRSA Antibiotic Resistance. *Cell* **2017**, *171*, 1354–1367.e20.

(6) Weihs, F.; Wacnik, K.; Turner, R. D.; Culley, S.; Henriques, R.; Foster, S. J. Heterogeneous Localisation of Membrane Proteins in Staphylococcus Aureus. *Sci Rep* **2018**, *8*, 3657.

(7) Hines, K. M.; Waalkes, A.; Penewit, K.; Holmes, E. A.; Salipante, S. J.; Werth, B. J.; Xu, L. Characterization of the Mechanisms of Daptomycin Resistance among Gram-Positive Bacterial Pathogens by Multidimensional Lipidomics. *mSphere* **2017**, *2*, e00492–17.

(8) Tague, E. D.; Woodall, B. M.; Harp, J. R.; Farmer, A. T.; Fozo, E. M.; Campagna, S. R. Expanding Lipidomics Coverage: Effective Ultra Performance Liquid Chromatography-High Resolution Mass Spectrometer Methods for Detection and Quantitation of Cardiolipin, Phosphatidylglycerol, and Lysyl-Phosphatidylglycerol. *Metabolomics* **2019**, *15*, 53.

(9) Miller, L. N.; Brewer, W. T.; Williams, J. D.; Fozo, E. M.; Calhoun, T. R. Second Harmonic Generation Spectroscopy of Membrane Probe Dynamics in Gram-Positive Bacteria. *Biophysical Journal* **2019**, *117*, 1419–1428.

(10) Denich, T. J.; Beaudette, L. A.; Lee, H.; Trevors, J. T. Effect of Selected Environmental and Physico-Chemical Factors on Bacterial Cytoplasmic Membranes. *Journal of Microbiological Methods* **2003**, *52*, 149–182.

(11) Barák, I.; Muchová, K. The Role of Lipid Domains in Bacterial Cell Processes. *International Journal of Molecular Sciences* **2013**, *14*, 4050–4065.

(12) Zhang, Y.-M.; Rock, C. O. Membrane Lipid Homeostasis in Bacteria. *Nat Rev Microbiol* **2008**, *6*, 222–233.

(13) Needham, B. D.; Trent, M. S. Fortifying the Barrier: The Impact of Lipid A Remodelling on Bacterial Pathogenesis. *Nat Rev Microbiol* **2013**, *11*, 467–481.

(14) Lee, T.-H.; Hofferek, V.; Separovic, F.; Reid, G. E.; Aguilar, M.-I. The Role of Bacterial Lipid Diversity and Membrane Properties in Modulating Antimicrobial Peptide Activity and Drug Resistance. *Current Opinion in Chemical Biology* **2019**, *52*, 85–92.

(15) Mishra, N. N.; Bayer, A. S. Correlation of Cell Membrane Lipid Profiles with Daptomycin Resistance in Methicillin-Resistant Staphylococcus Aureus. *Antimicrobial Agents and Chemotherapy* **2013**, *57*, 1082–1085.

(16) Smith, D.; Artursson, P.; Avdeef, A.; Di, L.; Ecker, G. F.; Faller, B.; Houston, J. B.; Kansy, M.; Kerns, E. H.; Krämer, S. D.; Lennernäs, H.; van de Waterbeemd, H.; Sugano, K.; Testa, B. Passive Lipoidal Diffusion and Carrier-Mediated Cell Uptake Are Both Important Mechanisms of Membrane Permeation in Drug Disposition. *Mol. Pharmaceutics* **2014**, *11*, 1727–1738.

(17) Shai, Y. Mode of Action of Membrane Active Antimicrobial Peptides. *Peptide Science* **2002**, *66*, 236–248.

(18) Torcato, I. M.; Huang, Y.-H.; Franquelim, H. G.; Gaspar, D. D.; Craik, D. J.; Castanho, M. A. R. B.; Henriques, S. T. The Antimicrobial Activity of Sub3 Is Dependent on Membrane Binding and Cell-Penetrating Ability. *ChemBioChem* **2013**, *14*, 2013–2022.

(19) Guilhelmelli, F.; Vilela, N.; Albuquerque, P.; Derengowski, L.; Silva-Pereira, I.; Kyaw, C. Antibiotic Development Challenges: The Various Mechanisms of Action of Antimicrobial Peptides and of Bacterial Resistance. *Frontiers in Microbiology* **2013**, *4*.

(20) Reynolds, P. E. Structure, Biochemistry and Mechanism of Action of Glycopeptide Antibiotics. *Eur. J. Clin. Microbiol. Infect. Dis.* **1989**, *8*, 943–950.

(21) Ferreira, R. J.; Kasson, P. M. Antibiotic Uptake Across Gram-Negative Outer Membranes: Better Predictions Towards Better Antibiotics. *ACS Infect. Dis.* **2019**, *5*, 2096–2104.

(22) Cama, J.; Henney, A. M.; Winterhalter, M. Breaching the Barrier: Quantifying Antibiotic Permeability across Gram-negative Bacterial Membranes. *Journal of Molecular Biology* **2019**, *431*, 3531–3546.

(23) Halder, S.; Yadav, K. K.; Sarkar, R.; Mukherjee, S.; Saha, P.; Haldar, S.; Karmakar, S.; Sen, T. Alteration of Zeta Potential and Membrane Permeability in Bacteria: A Study with Cationic Agents. *SpringerPlus* **2015**, *4*, 672.

(24) Aloia, R. C.; Boggs, J. M. *Membrane Fluidity in Biology: Cellular Aspects*; Academic Press, 2013.

(25) Kaneda, T. Iso- and Anteiso-Fatty Acids in Bacteria: Biosynthesis, Function, and Taxonomic Significance. *Microbiological Reviews* **1991**, *55*, 288–302.

(26) Nickels, J. D.; Chatterjee, S.; Mostofian, B.; Stanley, C. B.; Ohl, M.; Zolnierczuk, P.; Schulz, R.; Myles, D. A. A.; Standaert, R. F.; Elkins, J. G.; Cheng, X.; Katsaras, J. Bacillus Subtilis Lipid Extract, A Branched-Chain Fatty Acid Model Membrane. *J. Phys. Chem. Lett.* **2017**, *8*, 4214–4217.

(27) Cheng, J. T. J.; Hale, J. D.; Elliott, M.; Hancock, R. E. W.; Straus, S. K. The Importance of Bacterial Membrane Composition in the Structure and Function of Aurein 2.2 and Selected Variants. *Biochimica et Biophysica Acta (BBA) - Biomembranes* **2011**, *1808*, 622–633.

(28) Diomande, S.; NGUYEN-THE, C.; Guinebretière, M.-H.; Broussolle, V.; Brillard, J. Role of Fatty Acids in Bacillus Environmental Adaptation. *Frontiers in Microbiology* **2015**, *6*.

(29) Wydro, P.; Witkowska, K. The Interactions between Phosphatidylglycerol and Phosphatidylethanolamines in Model Bacterial Membranes: The Effect of the Acyl Chain Length and Saturation. *Colloids and Surfaces B: Biointerfaces* **2009**, *72*, 32–39.

(30) Carey, A. B.; Ashenden, A.; Köper, I. Model Architectures for Bacterial Membranes. *Biophys Rev* **2022**, *14*, 111–143.

(31) Luchini, A.; Cavasso, D.; Radulescu, A.; D'Errico, G.; Paduano, L.; Vitiello, G. Structural Organization of Cardiolipin-Containing Vesicles as Models of the Bacterial Cytoplasmic Membrane. *Langmuir* **2021**, *37*, 8508–8516.

(32) Menichetti, F. Current and Emerging Serious Gram-positive Infections. *Clinical Microbiology and Infection* **2005**, *11*, 22–28.

(33) Woodford, N.; Livermore, D. M. Infections Caused by Gram-positive Bacteria: A Review of the Global Challenge. *Journal of Infection* **2009**, *59*, S4–S16.

(34) Lipinski, C. A.; Lombardo, F.; Dominy, B. W.; Feeney, P. J. Experimental and Computational Approaches to Estimate Solubility and Permeability in Drug Discovery and Development Settings. *Advanced Drug Delivery Reviews* **2012**, *64*, 4–17.

(35) Grigor'eva, A.; Bardasheva, A.; Tupitsyna, A.; Amirkhanov, N.; Tikunova, N.; Pyshnyi, D.; Ryabchikova, E. Changes in the Ultrastructure of Staphylococcus Aureus Treated with Cationic Peptides and Chlorhexidine. *Microorganisms* **2020**, *8*, 1991.

(36) Matias, V. R. F.; Beveridge, T. J. Native Cell Wall Organization Shown by Cryo-Electron Microscopy Confirms the Existence of a Periplasmic Space in Staphylococcus Aureus. *J Bacteriol* **2006**, *188*, 1011–1021.

(37) Vazquez-Muñoz, R.; Meza-Villezcas, A.; Fournier, P. G. J.; Soria-Castro, E.; Juarez-Moreno, K.; Gallego-Hernández, A. L.; Bogdanchikova, N.; Vazquez-Duhalt, R.; Huerta-Saquero, A. Enhancement of Antibiotics Antimicrobial Activity Due to the Silver Nanoparticles Impact on the Cell Membrane. *PLOS ONE* **2019**, *14*, e0224904.

(38) Diestra, E.; Cayrol, B.; Arluison, V.; Risco, C. Cellular Electron Microscopy Imaging Reveals the Localization of the Hfq Protein Close to the Bacterial Membrane. *PLoS ONE* **2009**, *4*, e8301.

(39) Costerton, J. W. The Role of Electron Microscopy in the Elucidation of Bacterial Structure and Function. *Annual Review of Microbiology* **1979**, *33*, 459–479.

(40) Hartmann, M.; Berditsch, M.; Hawecker, J.; Ardakani, M. F.; Gerthsen, D.; Ulrich, A. S. Damage of the Bacterial Cell Envelope by Antimicrobial Peptides Gramicidin S and PGLa as Revealed by Transmission and Scanning Electron Microscopy. *Antimicrobial Agents and Chemotherapy* **2010**, *54*, 3132–3142.

(41) Wenzel, M.; Dekker, M. P.; Wang, B.; Burggraaf, M. J.; Bitter, W.; van Weering, J. R. T.; Hamoen, L. W. A Flat Embedding Method for Transmission Electron Microscopy Reveals an Unknown Mechanism of Tetracycline. *Commun Biol* **2021**, *4*, 1–13.

(42) Yusook, K.; Weeranantanapan, O.; Hua, Y.; Kumkrai, P.; Chudapongse, N. Lupinifolin from Derris Reticulata Possesses Bactericidal Activity on Staphylococcus Aureus by Disrupting Bacterial Cell Membrane. *J Nat Med* **2017**, *71*, 357–366.

(43) Appala, K.; Bimpeh, K.; Freeman, C.; Hines, K. M. Recent Applications of Mass Spectrometry in Bacterial Lipidomics. *Anal Bioanal Chem* **2020**, *412*, 5935–5943.

(44) Gidden, J.; Denson, J.; Liyanage, R.; Ivey, D. M.; Lay, J. O. Lipid Compositions in Escherichia Coli and Bacillus Subtilis during Growth as Determined by MALDI-TOF and TOF/TOF Mass Spectrometry. *International Journal of Mass Spectrometry* **2009**, *283*, 178–184.

(45) Boxer, S. G.; Kraft, M. L.; Weber, P. K. Advances in Imaging Secondary Ion Mass Spectrometry for Biological Samples. *Annual Review of Biophysics* **2009**, *38*, 53–74.

(46) Evason, D. J.; Claydon, M. A.; Gordon, D. B. Exploring the Limits of Bacterial Identification by Intact Cell-Mass Spectrometry. *J. Am. Soc. Mass Spectrom.* **2001**, *12*, 49–54.

(47) Kraft, M. L.; Klitzing, H. A. Imaging Lipids with Secondary Ion Mass Spectrometry. *Biochimica et Biophysica Acta (BBA) - Molecular and Cell Biology of Lipids* **2014**, *1841*, 1108–1119.

(48) Lanni, E. J.; Rubakhin, S. S.; Sweedler, J. V. Mass Spectrometry Imaging and Profiling of Single Cells. *Journal of Proteomics* **2012**, *75*, 5036–5051.

(49) Gibbs, K. A.; Isaac, D. D.; Xu, J.; Hendrix, R. W.; Silhavy, T. J.; Theriot, J. A. Complex Spatial Distribution and Dynamics of an Abundant Escherichia Coli Outer Membrane Protein, LamB. *Molecular Microbiology* **2004**, *53*, 1771–1783.

(50) Meyer, P.; Dworkin, J. Applications of Fluorescence Microscopy to Single Bacterial Cells. *Research in Microbiology* **2007**, *158*, 187–194.

(51) Pogliano, J.; Osborne, N.; Sharp, M. D.; Abanes-De Mello, A.; Perez, A.; Sun, Y.-L.; Pogliano, K. A Vital Stain for Studying Membrane Dynamics in Bacteria: A Novel Mechanism Controlling Septation during Bacillus Subtilis Sporulation. *Molecular Microbiology* **1999**, *31*, 1149–1159.

(52) Blake, M. J.; Colon, B. A.; Calhoun, T. R. Leaving the Limits of Linearity for Light Microscopy. *J. Phys. Chem. C* **2020**, *124*, 24555–24565.

(53) Allhusen, J. S.; Conboy, J. C. The Ins and Outs of Lipid Flip-Flop. *Acc. Chem. Res.* **2017**, *50*, 58–65.

(54) Rokitskaya, T. I.; Aleksandrova, E. V.; Korshunova, G. A.; Khailova, L. S.; Tashlitsky, V. N.; Luzhkov, V. B.; Antonenko, Y. N. Membrane Permeability of Modified Butyltriphenylphosphonium Cations. *J. Phys. Chem. B* **2022**, *126*, 412–422.

(55) McConnell, H. M.; Kornberg, R. D. Inside-Outside Transitions of Phospholipids in Vesicle Membranes. *Biochemistry* **1971**, *10*, 1111–1120.

(56) Homan, R.; Pownall, H. J. Transbilayer Diffusion of Phospholipids: Dependence on Headgroup Structure and Acyl Chain Length. *Biochimica et Biophysica Acta (BBA) - Biomembranes* **1988**, *938*, 155–166.

(57) Kleinfeld, A. M.; Chu, P.; Storch, J. Flip-Flop Is Slow and Rate Limiting for the Movement of Long Chain Anthroyloxy Fatty Acids across Lipid Vesicles. *Biochemistry* **1997**, *36*, 5702–5711.

(58) Moreno, M. J.; Estronca, L. M. B. B.; Vaz, W. L. C. Translocation of Phospholipids and Dithionite Permeability in Liquid-Ordered and Liquid-Disordered Membranes. *Biophysical Journal* **2006**, *91*, 873–881.

(59) Liu, J.; Conboy, J. C. 1,2-Diacyl-Phosphatidylcholine Flip-Flop Measured Directly by Sum-Frequency Vibrational Spectroscopy. *Biophysical Journal* **2005**, *89*, 2522–2532.

(60) Anglin, T. C.; Conboy, J. C. Kinetics and Thermodynamics of Flip-Flop in Binary Phospholipid Membranes Measured by Sum-Frequency Vibrational Spectroscopy. *Biochemistry* **2009**, *48*, 10220–10234.

(61) Regev, R.; Yeheskely-Hayon, D.; Katzir, H.; Eytan, G. D. Transport of Anthracyclines and Mitoxantrone across Membranes by a Flip-Flop Mechanism. *Biochemical Pharmacology* **2005**, *70*, 161–169.

(62) Róg, T.; Stimson, L. M.; Pasenkiewicz-Gierula, M.; Vattulainen, I.; Karttunen, M. Replacing the Cholesterol Hydroxyl Group with the Ketone Group Facilitates Sterol Flip-Flop and Promotes Membrane Fluidity. *J. Phys. Chem. B* **2008**, *112*, 1946–1952.

(63) Parisio, G.; Sperotto, M. M.; Ferrarini, A. Flip-Flop of Steroids in Phospholipid Bilayers: Effects of the Chemical Structure on Transbilayer Diffusion. *J. Am. Chem. Soc.* **2012**, *134*, 12198–12208.

(64) Rokitskaya, T. I.; Korshunova, G. A.; Antonenko, Y. N. Effect of Alkyl Chain Length on Translocation of Rhodamine B N-Alkyl Esters across Lipid Membranes. *Biophysical Journal* **2018**, *115*, 514–521.

(65) Rokitskaya, T. I.; B. Luzhkov, V.; A. Korshunova, G.; N. Tashlitsky, V.; N. Antonenko, Y. Effect of Methyl and Halogen Substituents on the Transmembrane Movement of Lipophilic Ions. *Physical Chemistry Chemical Physics* **2019**, *21*, 23355–23363.

(66) Kamp, F.; Zakim, D.; Zhang, F.; Noy, N.; Hamilton, J. A. Fatty Acid Flip-Flop in Phospholipid Bilayers Is Extremely Fast. *Biochemistry* **1995**, *34*, 11928–11937.

(67) Armstrong, V. T.; Brzustowicz, M. R.; Wassall, S. R.; Jenski, L. J.; Stillwell, W. Rapid Flip-Flop in Polyunsaturated (Docosahexaenoate) Phospholipid Membranes. *Archives of Biochemistry and Biophysics* **2003**, *414*, 74–82.

(68) López-Lara, I. M.; Geiger, O. Bacterial Lipid Diversity. *Biochimica et Biophysica Acta (BBA) - Molecular and Cell Biology of Lipids* **2017**, *1862*, 1287–1299.

(69) Gonella, G.; Dai, H.-L. Second Harmonic Light Scattering from the Surface of Colloidal Objects: Theory and Applications. *Langmuir* **2014**, *30*, 2588–2599.

(70) Moreaux, L.; Sandre, O.; Mertz, J. Membrane Imaging by Second-Harmonic Generation Microscopy. *J. Opt. Soc. Am. B, JOSAB* **2000**, *17*, 1685–1694.

(71) Nguyen, T. T.; Conboy, J. C. High-Throughput Screening of Drug–Lipid Membrane Interactions via Counter-Propagating Second Harmonic Generation Imaging. *Anal. Chem.* **2011**, *83*, 5979–5988.

(72) Kumal, R. R.; Nguyenhuu, H.; Winter, J. E.; McCarley, R. L.; Haber, L. H. Impacts of Salt, Buffer, and Lipid Nature on Molecular Adsorption and Transport in Liposomes As Observed by Second Harmonic Generation. *J. Phys. Chem. C* **2017**, *121*, 15851–15860.

(73) Dikkumbura, A. S.; Aucoin, A. V.; Ali, R. O.; Dalier, A.; Gilbert, D. W.; Schneider, G. J.; Haber, L. H. Influence of Acetaminophen on Molecular Adsorption and Transport Properties at Colloidal Liposome Surfaces Studied by Second Harmonic Generation Spectroscopy. *Langmuir* **2022**, *38*, 3852–3859.

(74) Hamal, P.; Nguyenhuu, H.; Subasinghege Don, V.; Kumal, R. R.; Kumar, R.; McCarley, R. L.; Haber, L. H. Molecular Adsorption and Transport at Liposome Surfaces

Studied by Molecular Dynamics Simulations and Second Harmonic Generation Spectroscopy. *J. Phys. Chem. B* **2019**, *123*, 7722–7730.

(75) Yan, E. C. Y.; Eisenthal, K. B. Effect of Cholesterol on Molecular Transport of Organic Cations across Liposome Bilayers Probed by Second Harmonic Generation. *Biophysical Journal* **2000**, *79*, 898–903.

(76) Hamal, P.; Subasinghege Don, V.; Nguyenhuu, H.; Ranasinghe, J. C.; Nauman, J. A.; McCarley, R. L.; Kumar, R.; Haber, L. H. Influence of Temperature on Molecular Adsorption and Transport at Liposome Surfaces Studied by Molecular Dynamics Simulations and Second Harmonic Generation Spectroscopy. *J. Phys. Chem. B* **2021**, *125*, 10506–10513.

(77) Srivastava, A.; Eisenthal, K. B. Kinetics of Molecular Transport across a Liposome Bilayer. *Chemical Physics Letters* **1998**, *292*, 345–351.

(78) Ruan, Y.; Guha, P.; Chen, S.-L.; Yuan, Q.; Gan, W. Observing the Structural Variations on Binary Complex Vesicle Surfaces and the Influence on Molecular Transportation. *Chemical Physics* **2021**, *548*, 111250.

(79) Chen, S. L.; Liang, Y. Z.; Hou, Y.; Wang, H.; Wu, X.; Gan, W.; Yuan, Q. Simple Physics in and Easy Manipulating of the Interfacial Behavior of Charged Molecules on Drug Delivery Vesicles. *Materials Today Physics* **2019**, *9*, 100092.

(80) Hou, Y.; Chen, S.-L.; Gan, W.; Ma, X.; Yuan, Q. Understanding the Dynamic Behavior of an Anticancer Drug, Doxorubicin, on a Lipid Membrane Using Multiple Spectroscopic Techniques. *J. Phys. Chem. B* **2019**, *123*, 3756–3762.

(81) Li, B.; Li, J.; Gan, W.; Tan, Y.; Yuan, Q. Unveiling the Molecular Dynamics in a Living Cell to the Subcellular Organelle Level Using Second-Harmonic Generation Spectroscopy and Microscopy. *Anal. Chem.* **2021**, *93*, 14146–14152.

(82) Campagnola, P. J.; Wei, M.-d.; Lewis, A.; Loew, L. M. High-Resolution Nonlinear Optical Imaging of Live Cells by Second Harmonic Generation. *Biophysical Journal* **1999**, *77*, 3341–3349.

(83) Sharifian Gh., M.; Wilhelm, M. J.; Moore, M.; Dai, H.-L. Spatially Resolved Membrane Transport in a Single Cell Imaged by Second Harmonic Light Scattering. *Biochemistry* **2019**, *58*, 1841–1844.

(84) Zeng, J.; Eckenrode, H. M.; Dai, H.-L.; Wilhelm, M. J. Adsorption and Transport of Charged vs. Neutral Hydrophobic Molecules at the Membrane of Murine Erythroleukemia (MEL) Cells. *Colloids and Surfaces B: Biointerfaces* **2015**, *127*, 122–129.

(85) Moen, E. K.; Ibey, B. L.; Beier, H. T. Detecting Subtle Plasma Membrane Perturbation in Living Cells Using Second Harmonic Generation Imaging. *Biophysical Journal* **2014**, *106*, L37–L40.

(86) Miller, L. N.; Blake, M. J.; Page, E. F.; Castillo, H. B.; Calhoun, T. R. Phosphate Ions Alter the Binding of Daptomycin to Living Bacterial Cell Surfaces. *ACS Infect. Dis.* **2021**,

(87) Zeng, J.; Eckenrode, H. M.; Dounce, S. M.; Dai, H.-L. Time-Resolved Molecular Transport across Living Cell Membranes. *Biophysical Journal* **2013**, *104*, 139–145.

(88) Wu, T.; Wilhelm, M. J.; Li, Y.; Ma, J.; Dai, H.-L. Indole Facilitates Antimicrobial Uptake in Bacteria. *ACS Infect. Dis.* **2022**,

(89) Wilhelm, M. J.; Sharifian Gh., M.; Wu, T.; Li, Y.; Chang, C.-M.; Ma, J.; Dai, H.-L. Determination of Bacterial Surface Charge Density via Saturation of Adsorbed Ions. *Biophysical Journal* **2021**, *120*, 2461–2470.

(90) Wilhelm, M. J.; Dai, H.-L. Molecule-Membrane Interactions in Biological Cells Studied

with Second Harmonic Light Scattering. *Chemistry – An Asian Journal* **2020**, *15*, 200–213.

(91) Wilhelm, M. J.; Sharifian Gh., M.; Dai, H.-L. Influence of Molecular Structure on Passive Membrane Transport: A Case Study by Second Harmonic Light Scattering. *J. Chem. Phys.* **2019**, *150*, 104705.

(92) Sharifian Gh., M.; Wilhelm, M. J.; Dai, H.-L. Azithromycin-Induced Changes to Bacterial Membrane Properties Monitored in Vitro by Second-Harmonic Light Scattering. *ACS Med Chem Lett* **2018**, *9*, 569–574.

(93) Sharifian Gh., M.; Wilhelm, M. J.; Dai, H.-L. Label-Free Optical Method for Quantifying Molecular Transport Across Cellular Membranes In Vitro. *J. Phys. Chem. Lett.* **2016**, *7*, 3406–3411.

(94) Wilhelm, M. J.; Sharifian Gh., M.; Dai, H.-L. Chemically Induced Changes to Membrane Permeability in Living Cells Probed with Nonlinear Light Scattering. *Biochemistry* **2015**, *54*, 4427–4430.

(95) Wilhelm, M. J.; Sheffield, J. B.; Sharifian Gh., M.; Wu, Y.; Spahr, C.; Gonella, G.; Xu, B.; Dai, H.-L. Gram's Stain Does Not Cross the Bacterial Cytoplasmic Membrane. *ACS Chem. Biol.* **2015**, *10*, 1711–1717.

(96) Wilhelm, M. J.; Sheffield, J. B.; Gonella, G.; Wu, Y.; Spahr, C.; Zeng, J.; Xu, B.; Dai, H.-L. Real-Time Molecular Uptake and Membrane-Specific Transport in Living Cells by Optical Microscopy and Nonlinear Light Scattering. *Chemical Physics Letters* **2014**, *605–606*, 158–163.

(97) Kleinzeller, A. Ernest Overton's Contribution to the Cell Membrane Concept: A Centennial Appreciation. *Physiology* **1997**, *12*, 49–53.

(98) Missner, A.; Pohl, P. 110 Years of the Meyer–Overton Rule: Predicting Membrane Permeability of Gases and Other Small Compounds. *ChemPhysChem* **2009**, *10*, 1405–1414.

(99) Chopra, I.; Roberts, M. Tetracycline Antibiotics: Mode of Action, Applications, Molecular Biology, and Epidemiology of Bacterial Resistance. *Microbiology and Molecular Biology Reviews* **2001**, *65*, 232–260.

(100) Peter, S.; Alven, S.; Maseko, R. B.; Aderibigbe, B. A. Doxorubicin-Based Hybrid Compounds as Potential Anticancer Agents: A Review. *Molecules* **2022**, *27*, 4478.

(101) Wu, Y.; Yeh, F. L.; Mao, F.; Chapman, E. R. Biophysical Characterization of Styryl Dye-Membrane Interactions. *Biophysical Journal* **2009**, *97*, 101–109.

(102) Gaffield, M. A.; Betz, W. J. Imaging Synaptic Vesicle Exocytosis and Endocytosis with FM Dyes. *Nat Protoc* **2006**, *1*, 2916–2921.

(103) Schildkraut, J. S.; Penner, T. L.; Willand, C. S.; Ulman, A. Absorption and Second-Harmonic Generation of Monomer and Aggregate Hemicyanine Dye in Langmuir–Blodgett Films. *Opt. Lett., OL* **1988**, *13*, 134–136.

(104) Steinhoff, R.; Chi, L. F.; Marowsky, G.; Möbius, D. Protonation and Monolayer Aggregation Studied by Second-Harmonic Generation. *J. Opt. Soc. Am. B, JOSAB* **1989**, *6*, 843–847.

(105) Frallicciardi, J.; Melcr, J.; Siginou, P.; Marrink, S. J.; Poolman, B. Membrane Thickness, Lipid Phase and Sterol Type Are Determining Factors in the Permeability of Membranes to Small Solutes. *Nat Commun* **2022**, *13*, 1605.

(106) Matias, V. R. F.; Beveridge, T. J. Cryo-Electron Microscopy Reveals Native Polymeric Cell Wall Structure in Bacillus Subtilis 168 and the Existence of a Periplasmic Space. *Molecular Microbiology* **2005**, *56*, 240–251.

(107) Strahl, H.; Bürmann, F.; Hamoen, L. W. The Actin Homologue MreB Organizes the Bacterial Cell Membrane. *Nat Commun* **2014**, *5*, 3442.

(108) Lopez, D.; Koch, G. Exploring Functional Membrane Microdomains in Bacteria: An Overview. *Current Opinion in Microbiology* **2017**, *36*, 76–84.

(109) Sen, S.; Sirobhushanam, S.; Johnson, S. R.; Song, Y.; Tefft, R.; Gatto, C.; Wilkinson, B. J. Growth-Environment Dependent Modulation of Staphylococcus Aureus Branched-Chain to Straight-Chain Fatty Acid Ratio and Incorporation of Unsaturated Fatty Acids. *PLOS ONE* **2016**, *11*, e0165300.

(110) Kaneda, T. Fatty Acids of the Genus Bacillus: An Example of Branched-Chain Preference. *Bacteriol Rev* **1977**, *41*, 391–418.

(111) Wang, H.; Yan, E. C. Y.; Borguet, E.; Eisenthal, K. B. Second Harmonic Generation from the Surface of Centrosymmetric Particles in Bulk Solution. *Chemical Physics Letters* **1996**, *259*, 15–20.

(112) Park, J. H.; Sut, T. N.; Jackman, J. A.; Ferhan, A. R.; Yoon, B. K.; Cho, N.-J. Controlling Adsorption and Passivation Properties of Bovine Serum Albumin on Silica Surfaces by Ionic Strength Modulation and Cross-Linking. *Phys. Chem. Chem. Phys.* **2017**, *19*, 8854–8865.

(113) Doughty, B.; Rao, Y.; Kazer, S. W.; Kwok, S. J. J.; Turro, N. J.; Eisenthal, K. B. Binding of the Anti-Cancer Drug Daunomycin to DNA Probed by Second Harmonic Generation. *J. Phys. Chem. B* **2013**, *117*, 15285–15289.

(114) Nguyen, T. T.; Sly, K. L.; Conboy, J. C. Comparison of the Energetics of Avidin, Streptavidin, NeutrAvidin, and Anti-Biotin Antibody Binding to Biotinylated Lipid Bilayer Examined by Second-Harmonic Generation. *Anal. Chem.* **2012**, *84*, 201–208.